CrossMark

XMM and NuSTAR Observations of an Optically Quiescent Quasar

Claire Greenwell[1,2] , Poshak Gandhi[1] , George Lansbury[2] , Peter Boorman[1,3] , Vincenzo Mainieri[2] , and Daniel Stern[4]
[1] School of Physics & Astronomy, University of Southampton, Highfield, Southampton SO17 1BJ, UK; cgreenwell11@gmail.com
[2] European Southern Observatory, Karl-Schwarzschild-Strasse 2, D-85748, Germany
[3] Astronomical Institute, Academy of Sciences, Boční II 1401, CZ-14131 Prague, Czech Republic
[4] Jet Propulsion Laboratory, California Institute of Technology, 4800 Oak Grove Drive, Mail Stop 169-221, Pasadena, CA 91109, USA

Abstract

Optically quiescent quasars (OQQs) represent a recently systematized class of infrared-luminous active galactic nuclei (AGNs) that have galaxy-like optical continua. They may represent an interesting, brief phase in the AGN life cycle, e.g., either cocooned within high-covering-factor media or indicative of recent triggering, though their nature remains unclear. Here, we present the first targeted simultaneous X-ray observations of an OQQ, our previously identified prototype, SDSS J075139.06+402811.2 at $z = 0.587$. The source is significantly detected over 0.5–16 keV with XMM-Newton and NuSTAR, unambiguously confirming the presence of current accretion activity. Spectral modeling yields an intrinsic luminosity $L_{2-10\,\mathrm{keV}} \approx 4.4 \times 10^{43}$ erg s^{-1}, well within the AGN regime, but underluminous relative to its infrared power. It is lightly obscured, with log N_H [cm^{-2}] ≈ 22.

1. Introduction

Knowledge of the demographics of the active galactic nuclei (AGNs) population is essential to our understanding of how they evolve and influence their host galaxies. The majority of AGNs are affected by obscuration, which hides central AGN signatures (e.g., Ananna et al. 2020). This obscuration can take many forms, both stable (resulting in diverse AGN classes, e.g., Seyfert 1, Seyfert 2; Padovani et al. 2017), and transient (some "changing" look AGNs (CLAGNs); e.g., Risaliti et al. 2005; Ricci et al. 2016). CLAGNs can also present with a change in intrinsic flux, likely due to a change in accretion state (e.g., Stern et al. 2018). Selecting an unbiased sample of AGNs across these properties is challenging (e.g., Hickox & Alexander 2018; Asmus et al. 2020), and in this work, we address a gap in current samples that could represent an interesting and unusual phase of obscuration.

AGN selection in each portion of the electromagnetic spectrum has both advantages and drawbacks (Brandt & Alexander 2015; Padovani et al. 2017). Optical selection, using typical AGN emission lines, can miss heavily obscured or intrinsically faint objects (Hickox & Alexander 2018). Infrared (IR) selection offers the chance to investigate AGNs without optical signatures—the majority of IR emission from AGNs is reprocessed in dusty regions and therefore relatively unbiased (Gandhi et al. 2009; Asmus et al. 2015). Multiwavelength studies using combinations of large surveys can be used to select AGNs with interesting properties; furthermore, extreme, unusual objects can be found in these vast data sets.

To systematically search for AGNs with rare properties, we began an investigation based on bright, AGN-colored IR sources from WISE (Wright et al. 2010) with no clear optical signatures of AGN presence—specifically the [O III] λ5007 Å forbidden line, among the strongest lines found in the narrow-

line regions of AGNs. This optical–IR disparity would set any such AGNs apart from standard selection techniques. We designate such sources as "Optically Quiescent Quasars (OQQs)". Source powers were chosen to lie in the quasar regime in order to mitigate host-galaxy dilution (Moran et al. 2002) as a possible cause of the lack of optical emission lines. An in-depth study of a single, prototypical OQQ was presented in Greenwell et al. (2021), and this paper demonstrates how X-ray observations provide an important tool for analyzing the intrinsic emission of AGNs—particularly in the case of AGNs with atypical properties. The results from our full survey will be discussed in detail in C. Greenwell et al. (2022, in preparation).

Two likely physical scenarios that may explain the observed properties of OQQs are:

1. "Cocooned" AGN—the optical emission lines are not seen because the AGN is completely enshrouded in a (presumably transient) "cocoon" of gas and dust.
2. "Young" AGN—the AGN has recently switched on and has not yet ionized the narrow-line region (NLR): no [O III] line has yet been excited.

Both scenarios are interesting from an evolutionary perspective. AGN growth within fully enshrouding cocoons is suggested by some models (Fabian 1999), and OQQs would represent a systematic search for this class of source, though such candidates appear in various prior subsamples (e.g., Gandhi et al. 2002; Hviding et al. 2018). Similarly, in the young AGN scenario, it may be possible to constrain the duty cycle of NLR excitation (Schawinski et al. 2015; Gezari et al. 2017). However, the foremost requirement is an independent confirmation of the AGN nature of OQQs. This is especially important in the absence of optical AGN spectral signatures, and this is what we present herein.

2. Data

In order to (a) confirm the presence of an AGN and (b) constrain its spectral properties, the optimal tracer is X-ray
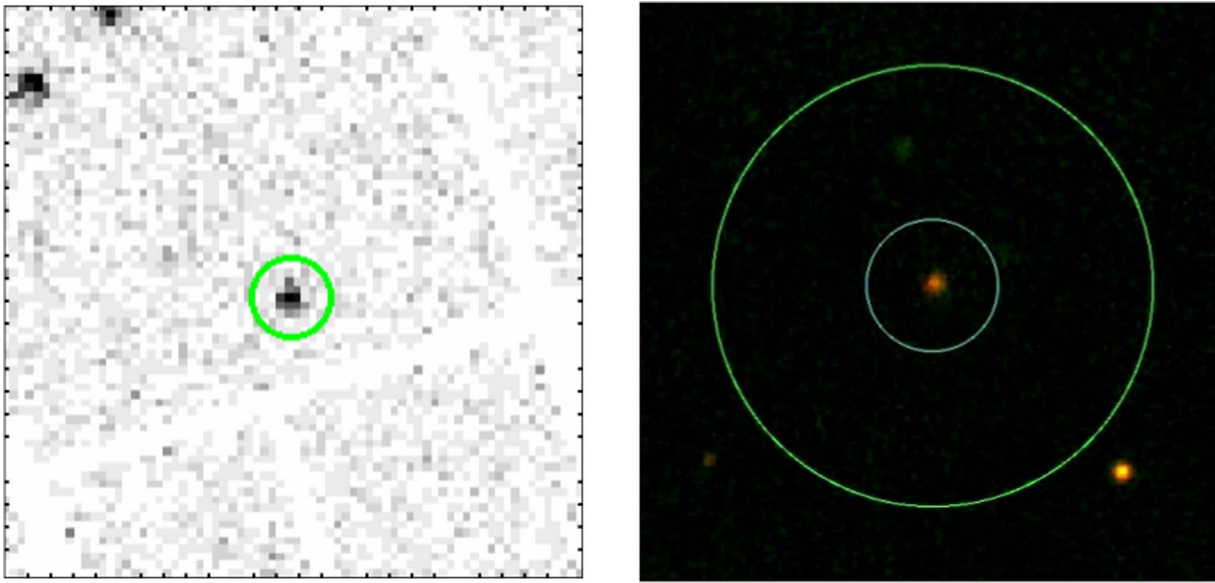
Figure 1. (left) XMM-Newton pn image; (right) PanSTARRS *irg* bands converted to RGB image. Green circles have a 20″ radius, and the cyan circle has a 6″ radius; all are centered on the optical source coordinates.

emission. Luminous, nuclear X-ray radiation is unlikely to originate from any source other than an AGN—intense star formation may produce (weaker) X-rays, but given the optically quiescent nature of OQQs ($<0.4\ M_\odot$ per year, stellar mass $\sim 10^{11} M_\odot$; Greenwell et al. 2021), sufficient star formation processes are not likely. XMM-Newton provides good angular resolution and sensitivity, ideal to examine the soft X-rays. NuSTAR (Harrison et al. 2013) looks at the harder X-rays, allowing us to measure the intrinsic X-ray luminosity if SDSS J075139.06+402811.2 (hereafter OQQ J0751+4028) proves to be heavily obscured. Based on the IR–X-ray relationship (Asmus et al. 2015; Stern 2015), we predict that OQQ J0751+4028 should be easily detected (under the assumption that it is indeed an AGN and not heavily Compton thick, at $z = 0.587$, $L_{2-10\,\mathrm{keV}}^{\mathrm{predicted}} {\sim} 2.6 \times 10^{44}$ erg s^{-1}), and analysis of its properties should be possible.

This analysis uses the following coordinated observations:

1. NuSTAR OBSID 60701009002: 50.6 ks, 2021 September 25 (start time: 12:06:09)
2. XMM-Newton OBSID 0884080101: 36.9 ks[5] of exposure, 2021 September 25 (start time: 13:28:37)

The data were reduced using standard recommended selection criteria, including removal of appropriate background, using the XMM-Newton Science Analysis Software[6] and HEASoft.[7] The target was detected significantly with XMM-Newton pn, MOS1 and MOS2[8], and with NuSTAR FPMA.[9] Source extraction regions were circles with radii of 45″ and 20″ for NuSTAR and XMM-Newton respectively. Background regions were annuli with an inner radius of 100″, outer radius of 180″ (partially cutout to avoid a chip edge), and circles of radius 90″ for NuSTAR and XMM-Newton, respectively. In

optical data (PanSTARRS), it appears small and red, with no visible morphological disturbances (see Figure 1).

3. Methods

The data were fit within XSPEC (Arnaud 1996), v.12.12.0, with several models covering various types and structures of obscuration, with different levels of complexity. Relevant parameters were allowed to vary freely (although tied between data sets): normalization, Γ, and N_{H}.

Under the assumption that OQQ J0751+4028 is an obscured AGN, the most basic combination of models we might expect to make a reasonable fit to the data is an absorbed power law (photoelectric absorption at the source redshift and Compton scattering attenuating an intrinsic power law; see the top-left panel in Figure 2). This model can produce an acceptable fit to the data, with light absorption (see Table 1). However, the best-fit $\Gamma = 1.08 \pm 0.16$ is unusually hard for an AGN compared to typical intrinsic spectral indices of $\Gamma \sim 1.9$ (Ricci et al. 2017a). There is some degeneracy between N_{H} and Γ values, so in order to investigate the likelihood of a more typical intrinsic AGN power law, we fit the same model, but with a fixed $\Gamma = 1.9$. This also produces an acceptable fit, with a slight increase in $\log(N_{\mathrm{H}}; \mathrm{cm}^{-2}) = 21.56$–22.30 (see Table 1).

Given the consistently hard Γ seen in the absorbed power-law model, we next investigate two more physically realistic models, which are still relatively simple: torus reprocessing (MYTORUS in coupled mode with covering factor fixed at 0.5; Murphy & Yaqoob 2009) and spherical obscuration (TRANS model from BNTORUS; Brightman & Nandra 2011, hereafter BNSPHERE).

BNSPHERE represents the physically expected obscuring structure around a "Cocooned" AGN. MYTORUS does not specifically allow full covering and is restricted to $\Gamma \geqslant 1.4$, higher than previously found Γ values. BNSPHERE is also limited, but to $\Gamma \geqslant 1.0$.

Other parameters are fixed to simplify the modeling. MYTORUS inclination was set to 90° (i.e., through the torus, to fit with our assumption of an obscured AGN). BNSPHERE iron and total elemental abundances were set to solar values.
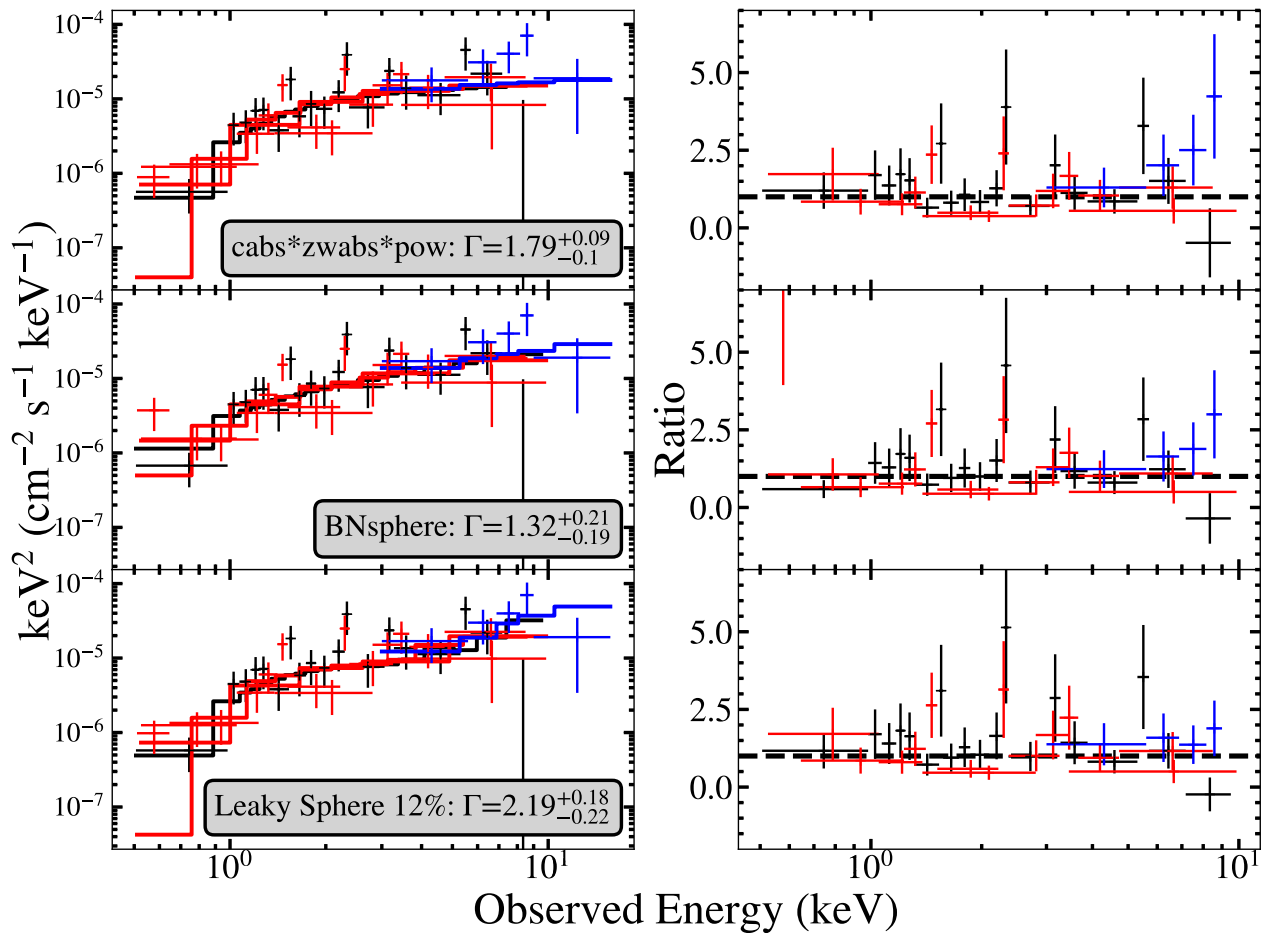
---

[5] After cleaning 16.4/28.3/29.3 ks on pn/MOS1/MOS2.
[6] http://xmm.esa.int/sas/
[7] https://heasarc.gsfc.nasa.gov/docs/nustar/analysis/
[8] 0.5–10 keV; net counts 87/36/65.
[9] 3–16 keV; net counts 55. Not detected in FPMB alone, due to higher background flux.

Figure 2. Spectra and ratio between data and model for (top) CABS∗ZWABS∗POW, $\Gamma = 1.79$; (middle) BNSPHERE, $\Gamma = 1.35$; (bottom) "leaky sphere", $\Gamma = 2.19$. Shown is XMM-Newton-pn (black), XMM-Newton-MOS (red), and NuSTAR FPMA (blue), binned to a minimum of 2 counts per bin.

The results for the models thus far consistently produce a hard Γ ($\lesssim 1.5$). This would be an unusual intrinsic value for an AGN and could indicate that we are underestimating the optical depth of the obscuration present in the system, a possibility also hinted at by the lower than expected luminosity. None of the models above can produce a $\log(N_H)$ greater than ~ 22.3, thus we propose an alternative: a thick spherical obscurer (represented in XSPEC with BNSPHERE) in tandem with a scattered fraction (CONSTANT) of the intrinsic power law (ZCUTOFFPL). The scattered fraction represents a "leak" through Compton-thin obscuration from an otherwise Compton-thick sphere. With this we can investigate higher N_H values while still providing a satisfactory fit to the softer X-rays, i.e., dominated by the scattered power law rather than a Compton hump. Here we show the results with scattering fraction fixed at 12%, which produces an intrinsic X-ray luminosity close to that predicted from the 12 μm luminosity.

Fixing the value of Γ makes a firm assumption about the nature of the intrinsic AGN emission, which we can make less stringent with Bayesian X-ray Analysis (BXA) (Buchner et al. 2014). We can include knowledge about the likely physical characteristics by selecting an appropriate prior: A Gaussian prior for Γ[10] is appropriate as it allows a physically motivated preference toward likely values and excludes unphysical values. We try (a) a loose Gaussian prior: $\Gamma = 2.0 \pm 0.3$; and

(b) a stricter Gaussian prior $\Gamma = 1.9 \pm 0.1$. As shown in Table 1, these both produce an acceptable fit to the data but struggle to produce a Γ value not unusually hard for an AGN. We can use the Bayesian evidence to compare the models and therefore determine which is most likely to have produced the observed data.

The final set of models we compare is (a) CABS∗ZWABS∗POW: with uniform, single value, and Gaussian priors on Γ; (b) MYTORUS; (c) BNSPHERE[11]; and (d) "leaky sphere".

4. Results

Across all models, the results show that the data can be explained by an obscured AGN. The parameters vary and in some cases may indicate unusual values, but all are consistent with the presence of an AGN. Full results for all models are shown in Table 1. None of the first six models show significant residuals, except possibly toward the hard end, and all are reasonable fits to the data (see Figure 2).

The preferred solution according to the Bayes factors is BNSPHERE (Table 1).[12] Comparison of (a) BNSPHERE and (b) "leaky sphere" (scattering fraction 12%) shows that LS is not

---

[10] N_H and normalization have log uniform priors.

[11] BNTORUS is known to have inaccuracies in the reflected component (e.g., Baloković et al. 2018); here we only consider the spherical component with no opening angle, which should not be affected.

[12] CABS∗ZWABS∗POW with a uniform prior fit is discarded from this point; the lack of constraint allows values of Γ that are not physically likely.

Table 1
Spectral Modeling Results

Model	Γ Prior	Γ	$\log N_{\rm H}$ (cm^{-2})	$\log N_{\rm H,\ sphere}$ (cm^{-2})	$\log L_{2-10\,\mathrm{keV}}$ ($\mathrm{erg\ s}^{-1}$)	cstat/d.o.f.	Bayes Factor (Normalized)
(1)	(2)	(3)	(4)	(5)	(6)	(7)	(8)
CABS*ZWABS*POW	Uniform	$0.98^{+0.18}_{-0.09}$	$21.62^{+0.27}_{-0.44}$		43.64 ± 0.04	334.1/377	⋯
CABS*ZWABS*POW	Fixed 1.9	1.90	$22.30^{+0.08}_{-0.11}$		43.68 ± 0.05	346.2/378	31.6
CABS*ZWABS*POW	1.9 ± 0.1	$1.79^{+0.09}_{-0.10}$	$22.26^{+0.08}_{-0.13}$		43.67 ± 0.05	337.7/377	12.6
CABS*ZWABS*POW	2.0 ± 0.3	$1.26^{+0.25}_{-0.16}$	$22.03^{+0.15}_{-0.41}$		43.64 ± 0.05	334.1/377	1.6
MYTORUS	2.0 ± 0.3	$1.47^{+0.17}_{-0.08}$	$22.05^{+0.12}_{-0.00}$		43.65 ± 0.04	336.6/377	2.0
BNSPHERE	2.0 ± 0.3	$1.32^{+0.21}_{-0.19}$	$21.95^{+0.15}_{-0.36}$		43.64 ± 0.05	334.1/377	best (≡1.0)
"leaky sphere", 12%	2.0 ± 0.3	$2.19^{-0.18}_{-0.22}$	$22.26^{-0.10}_{-0.17}$	$24.08^{-0.14}_{-0.14}$	44.45 ± 0.09	341.9/376	6.3

Note. Column details: (1) XSPEC model; (2) Γ prior; (3) Γ; (4) $N_{\rm H}$; (5) "sphere" $N_{\rm H}$; (6) unabsorbed 2–10 keV luminosity; (7) fit statistic; (8) Bayes factor compared to BNSPHERE.

favored. However, it is also not strongly counterindicated (i.e., the relative Bayes factor is low[13]).

BNSPHERE returns a preferred $\Gamma = 1.32^{+0.21}_{-0.19}$—unusually hard but not impossible for an AGN (e.g., Ricci et al. 2017a) —and $\log (N_{\rm H}/\mathrm{cm}^{-2}) = 21.95$ (see Figure 3). Forcing Γ to a more typical AGN value of 1.9 increases the $\log(N_{\rm H}/\mathrm{cm}^{-2})$ slightly to 22.3 but does not significantly affect the intrinsic luminosity (see Figure 3). The 12% "leaky sphere" model produces a softer Γ and, if closer to the truth, may imply a luminosity much closer to that expected.

That BNSPHERE is a reasonable fit to the data implies that the "cocooned AGN" scenario may be a feasible explanation for the observed properties. Obscuring material relatively close to the AGN may prevent ionizing radiation from within reaching farther out, and thus no narrow [O III] emission. We can also consider a situation where the NLR exists within a cocoon on intermediate scales between the torus and the inner galaxy (perhaps $\sim$ tens of parsecs), just large enough to cocoon the inner NLR. Depending on the gas-to-dust ratio in the obscuring material, relatively thin columns may be sufficient to extinct any [O III]. Based on the [O III] deficit between the general OQQ population and QSO2s (C. Greenwell et al. 2022, in preparation), a median $A_{\rm V} = 4.7$ mag is sufficient to extinct the theoretical [O III] line. This is equivalent to an NLR-obscuring neutral gas column density of $\log(N_{\rm H}/\mathrm{cm}^{-2}) \sim 22.8$ (assuming gas-to-dust ratios in AGN environments from Maiolino et al. 2001). This is higher than found in this analysis; however, the NLR-obscuring column is distinct from the line-of-sight X-ray-obscuring column, which may explain this difference.

The Fe Kα line (rest energy 6.4 keV) observed in many AGN spectra (e.g., Nandra 2006) originates from reprocessing of AGN emission in optically thick obscuring matter. For lightly obscured AGN, Shu et al. (2010) find a relationship between detected narrow Fe Kα EW and unabsorbed 2–10 keV luminosity[14], which we can use to roughly estimate an expected Fe Kα EW of 45 eV. We place an upper limit on the equivalent width (EW) of a putative narrow line by adding an unresolved Gaussian component to our transmission spectrum, with a width of 0.1 keV, finding an EW $\lesssim$ 26 eV— a low value that implies no line is likely to be present, further

reinforcing the conclusion that OQQ J0751+4028 is only lightly obscured.

The intrinsic rest frame 2–10 keV luminosity (according to BNSPHERE) is 4.39×10^{43} erg s^{-1}. The IR luminosity (1.30×10^{45} erg s^{-1} at 12 μm) of OQQ J0751+4028 implies a 2–10 keV luminosity of 2.61×10^{44} erg s^{-1} (from the 6 μm/ 2–10 keV relation; Stern 2015). Comparing these values, we find that the unabsorbed luminosity is $\sim$6 times lower than expected but still easily above the threshold of 10^{42}–10^{43} erg s^{-1} that is generally accepted for an AGN. In Figure 4 we compare the properties of OQQ J0751+4028 against a sample of Type 2 QSOs selected from SDSS with significant [O III] emission (QSO2s; Reyes et al. 2008; Yuan et al. 2016). Figure 4 shows that OQQ J0751+4028 lies below the IR-predicted values from Asmus et al. (2015) or Stern (2015), and also below the majority of QSO2s, which tend to fall closer to their predicted values. Figure 4 (right-hand panel) shows the measured X-ray luminosities of the QSO2s, along with the reported [O III]/X-ray relationship from Lamastra et al. (2009) —the majority of QSO2s lie close to the empirical prediction, but OQQ J0751+4028 is far from typical. Conversely, if we consider the "leaky sphere" model, the intrinsic X-ray luminosity may be closer to IR-predicted expectations (see Table 1); however, it would be further offset from the [O III]/ X-ray relationship.

5. Discussion

One important aim of this work is to place OQQ J0751+4028 (and in the future, its fellow OQQs) into context with the wider ranks of AGNs. We begin by considering what the results from this X-ray study allow us to infer about the intrinsic nature of this object. Crucially, the absorption-corrected luminosity shows that OQQ J0751+4028 is an AGN, regardless of the specific best-fit model that we adopt. This confirms the presence of ongoing accretion activity and gives credence to our IR selection, despite the apparent optical quiescence.

OQQ J0751+4028 must be obscured in X-rays, but is less likely to be Compton thick than thin. The Bayes factor for the highly obscured "leaky sphere" compared to the lightly obscured BNSPHERE is $\sim$6: a less likely fit but not decisively so. Recalling from the introduction our suggested scenarios regarding the nature of an optically quiescent AGN ("cocooned" and "young" AGN), we can only conclude at this stage that both remain possible. Nuclear optical extinction

---

[13] A value of 6.3 is "substantial evidence" in favor of BNSPHERE, but not decisive, according to the Jeffreys scale (Buchner et al. 2014).
[14] With large scatter, and from higher resolution Chandra data.
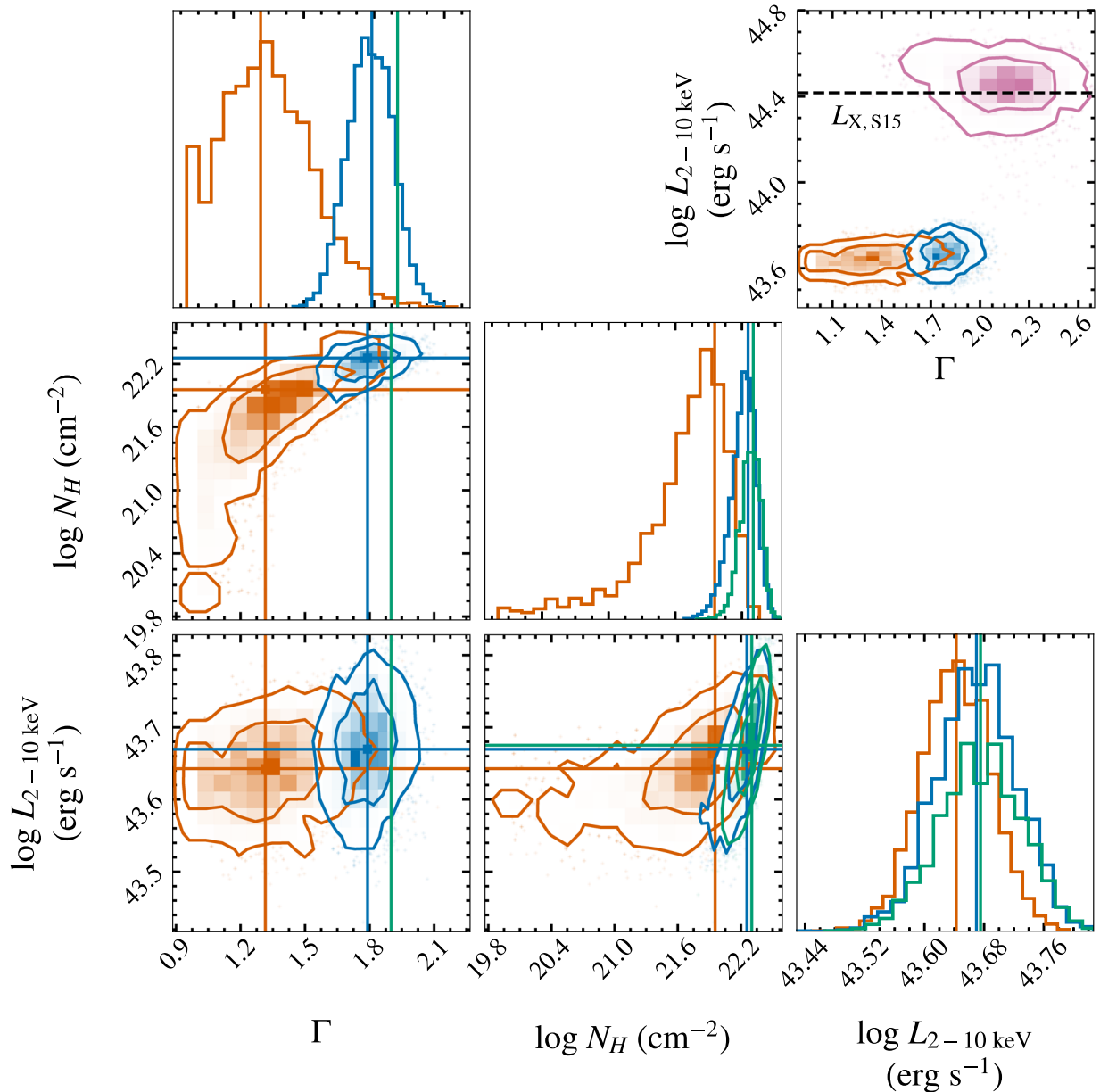
Figure 3. Corner plot of results with (a) CABS*ZWABS*POW, restrictive prior on Γ (blue); (b) BNSPHERE, physically representative prior on Γ (orange), and (c) CABS*ZWABS*POW, fixed $\Gamma = 1.9$ (green). Best-fit values for each parameter are shown with a solid line. (Top right) L_{2-10} vs. Γ contour with the IR-predicted luminosity shown (Stern 2015, dashed line)—the luminosity contours for the lightly obscured models are decisively below this level. Also shown are the results for the 12% scattered "leaky sphere", which is closer to predicted (pink).

is also required in both scenarios in order to hide the broad-line region, which we do not see.

The light obscuration we observe could be a more physically likely possibility for enshrouding material than optically thick material, supporting the idea of a "cocooned" AGN or similar to larger-scale host obscuration (e.g., Buchner & Bauer 2017). This interpretation could be consistent with a low intrinsic X-ray luminosity AGN if the Eddington ratio is low, as higher intensity AGNs are associated with lower covering factors (e.g., Ricci et al. 2017b).

An AGN in the process of switching on (a "young" AGN) might also show weak X-ray emission as it transitions to full accretion power. Kollatschny et al. (2020) present the opposite case—a switching-off AGN—in which they see a dramatic decrease in observed X-ray luminosity concurrent with a change in type from Seyfert 1 to 1.9 (i.e., a reduction in the broad emission lines but still with clear narrow lines). They find no evidence that this change is caused by absorption, indicating that it is an intrinsic luminosity change. Reversing this, we might expect to see the X-ray increase before the appearance of narrow lines.

Finally, we must consider the possibility that OQQ J0751+4028 is a fully "mature" AGN intrinsically lacking [O III]. Analysis of relationships between various emission-line properties of AGNs has shown that many of these properties are correlated (Eigenvector 1; Boroson & Green 1992). Shen & Ho (2014) show that the observed anticorrelation between [O III] and the relative strength of Fe II emission can be explained by changes in Eddington ratio; an AGN seen to lack [O III] could then be explained by a very high accretion rate. The higher Γ and intrinsic luminosities of the "Leaky Sphere" model may suggest this to be the case; however, a low
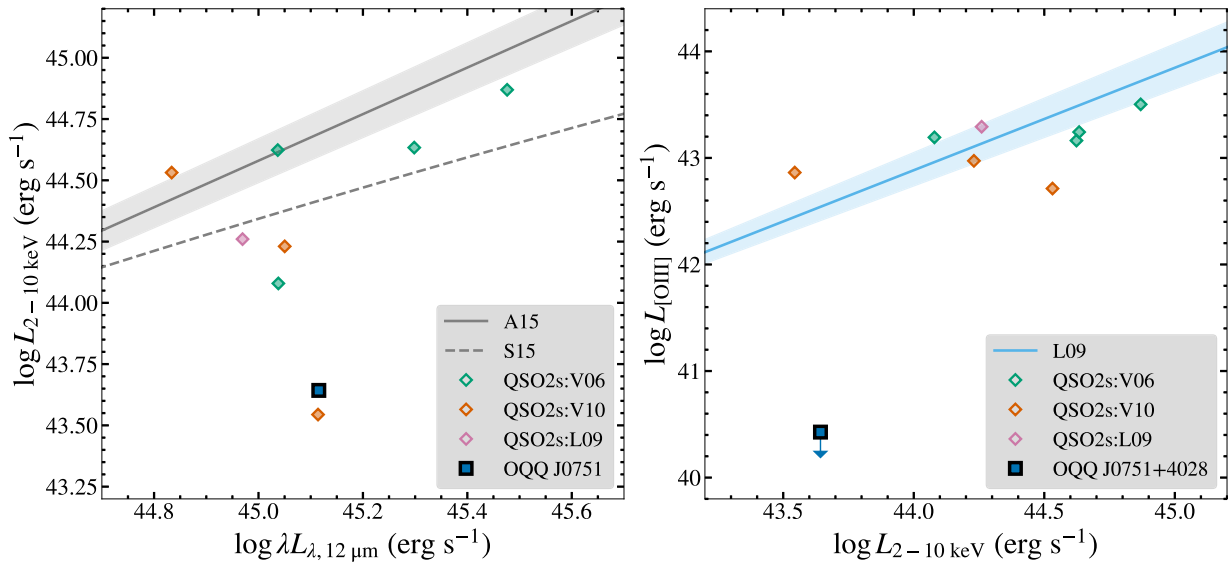
Figure 4. A comparison between OQQ J0751+4028 and QSO2s: (left) unabsorbed 2–10 keV luminosity against 12 μm luminosity. X-ray luminosities for QSO2s are from Vignali et al. (2006) (V06; green diamonds), Vignali et al. (2010) (V10; orange diamonds), and Lamastra et al. (2009) (L09; pink diamonds). Relationships from Asmus et al. (2015, A15) and Stern (2015, S15; 12 μm luminosities were converted to 6 μm luminosities using a relationship derived from the QSO template of Hao et al. 2007) are shown as gray lines. (right) Unabsorbed 2–10 keV luminosity against [O III] luminosity, with the relationship from Lamastra et al. (2009, L09).

"leak fraction" would be required and the fit statistics indicate this is unlikely. The stellar mass of OQQ J0751+4028, while uncertain, implies a high black hole mass ($\sim 5 \times 10^8 M_\odot$; Kormendy & Ho 2013) and, consequently, a very high luminosity to reach Eddington accretion levels—higher than seen in the WISE measurements.

OQQ-like objects are not new. For example, other groups of AGNs that have notable similarities to OQQs include weak-line quasars (WLQs) with weak X-ray emission and weak or absent emission lines (e.g., Wu et al. 2012), and X-ray bright, optically normal galaxies (XBONGs) selected as AGNs in X-rays, but showing no optical AGN signatures. In some cases, this is due to dilution by bright host galaxies of lower luminosity AGNs (Moran et al. 2002), in contrast to the OQQs, where AGN emission in the IR is bright, and dominates over their hosts.

Our OQQ selection is a first attempt to systematically search for this class of optically quiescent AGNs and our work unambiguously establishes that some AGNs can present bright ongoing nuclear accretion activity in X-rays yet show no signs of this in the optical. Details of our full sample will be presented in C. Greenwell et al. (2022, in preparation).

6. Summary

We present the first targeted, simultaneous, hard and soft X-ray observations of an optically quiescent quasar, demonstrating unequivocally that OQQ J0751+4028 is an AGN. It is lightly obscured ($N_H \approx 10^{22}$ cm^{-2}) and, while bright enough to confirm the presence of an AGN ($L_{2-10\,\mathrm{keV}} = 4.37 \times 10^{43}$ erg s^{-1}), our most likely model suggests it is less X-ray luminous than would be expected given its IR properties and in comparison to an [O III]-bright population. This result shows conclusively that the OQQ selection technique introduced in Greenwell et al. (2021), and discussed in depth in C. Greenwell et al. (2022, in preparation), can uncover previously unknown AGNs.

Appendix A
XSPEC Models

The models used in XSPEC are as follows:

1. Absorbed power law: CONSTANT∗PHABS∗CABS∗ZWABS∗ POW
2. MYTORUS: CONSTANT∗PHABS(ZPOWERLW∗ETABLE {MYTORUS_EZERO_V00.FITS} + CONSTANT∗ATABLE {MYTORUS_SCATTEREDH500_V00.FITS})
3. BNSPHERE: CONSTANT∗PHABS∗ATABLE{SPHERE0708.FITS}
4. "leaky sphere": CONSTANT∗PHABS∗(ATABLE{SPHERE0708. FITS}+CONSTANT∗ZWABS∗ZCUTOFFPL)
5. Absorbed power law with neutral iron line: CONSTANT∗- PHABS(CABS∗ZWABS∗POWERLAW+ZGAUSS).

All models include Galactic absorption (PHABS) of $N_{\rm H} = 5.6 \times 10^{20}$ cm^{-2} (HI4PI Collaboration et al. 2016). A cross-calibration constant of 0.93:1.02:0.98:1.00 (e.g., Madsen et al. 2015) was used for XMM-Newton(pn):XMM-Newton(MOS1): XMM-Newton(MOS2):NuSTAR; this was fixed because the observations were simultaneous. Spectra were binned to 3/1 counts per bin for NuSTAR/XMM-Newton and fit with `wstat` (Wachter et al. 1979)—the version of `cstat` (Cash 1979) used by XSPEC when a background is included: https://heasarc. gsfc.nasa.gov/xanadu/xspec/manual/node318.html#Appendix Statistics.

Appendix B
Data Availability

The optical and IR data underlying this article are publicly available from the WISE All-Sky Survey (doi:10.26131/IRSA1) and SDSS DR15. X-ray data are currently in the proprietary period but will become publicly available with the Observation IDs listed above.

ORCID iDs

Claire Greenwell ⦿ https://orcid.org/0000-0002-7719-5809
Poshak Gandhi ⦿ https://orcid.org/0000-0003-3105-2615
George Lansbury ⦿ https://orcid.org/0000-0002-5328-9827
Peter Boorman ⦿ https://orcid.org/0000-0001-9379-4716
Vincenzo Mainieri ⦿ https://orcid.org/0000-0002-1047-9583
Daniel Stern ⦿ https://orcid.org/0000-0003-2686-9241

References

Ananna, T. T., Treister, E., Urry, C. M., et al. 2020, ApJ, 889, 17
Arnaud, K. A. 1996, in ASP Conf. Ser. 101, Astronomical Data Analysis Software and Systems V, ed. G. H. Jacoby & J. Barnes (San Francisco, CA: ASP), 17
Asmus, D., Gandhi, P., Hönig, S. F., Smette, A., & Duschl, W. J. 2015, MNRAS, 454, 766
Asmus, D., Greenwell, C. L., Gandhi, P., et al. 2020, MNRAS, 494, 1784
Astropy Collaboration, Price-Whelan, A. M., Sipőcz, B. M., et al. 2018, AJ, 156, 123
Astropy Collaboration, Robitaille, T. P., Tollerud, E. J., et al. 2013, A&A, 558, A33
Baloković, M., Brightman, M., Harrison, F. A., et al. 2018, ApJ, 854, 42
Boroson, T. A., & Green, R. F. 1992, ApJS, 80, 109
Brandt, W. N., & Alexander, D. M. 2015, A&ARv, 23, 1
Brightman, M., & Nandra, K. 2011, MNRAS, 413, 1206
Buchner, J. 2021, JOSS, 6, 3001
Buchner, J., & Bauer, F. E. 2017, MNRAS, 465, 4348
Buchner, J., Georgakakis, A., Nandra, K., et al. 2014, A&A, 564, A125
Cash, W. 1979, ApJ, 228, 939
Fabian, A. C. 1999, MNRAS, 308, L39
Foreman-Mackey, D. 2016, JOSS, 1, 24
Gandhi, P., Crawford, C. S., & Fabian, A. C. 2002, MNRAS, 337, 781
Gandhi, P., Horst, H., Smette, A., et al. 2009, A&A, 502, 457
Gezari, S., Hung, T., Cenko, S. B., et al. 2017, ApJ, 835, 144
Greenwell, C., Gandhi, P., Stern, D., et al. 2021, MNRAS, 503, L80
Hao, L., Weedman, D. W., Spoon, H. W. W., et al. 2007, ApJ, 655, L77
Harrison, F. A., Craig, W. W., Christensen, F. E., et al. 2013, ApJ, 770, 103
Hickox, R. C., & Alexander, D. M. 2018, ARA&A, 56, 625
Hviding, R. E., Hickox, R. C., Hainline, K. N., et al. 2018, MNRAS, 474, 1955
HI4PI Collaboration, Ben Bekhti, N, Flöer, L., et al. 2016, A&A, 594, A116
Kollatschny, W., Grupe, D., Parker, M. L., et al. 2020, A&A, 638, A91
Kormendy, J., & Ho, L. C. 2013, ARA&A, 51, 511
Lamastra, A., Bianchi, S., Matt, G., et al. 2009, A&A, 504, 73
Madsen, K. K., Harrison, F. A., Markwardt, C. B., et al. 2015, ApJS, 220, 8
Maiolino, R., Marconi, A., Salvati, M., et al. 2001, A&A, 365, 28
Moran, E. C., Filippenko, A. V., & Chornock, R. 2002, ApJ, 579, L71
Murphy, K. D., & Yaqoob, T. 2009, MNRAS, 397, 1549
Nandra, K. 2006, MNRAS, 368, L62
Padovani, P., Alexander, D. M., Assef, R. J., et al. 2017, A&ARv, 25, 2
Reyes, R., Zakamska, N. L., Strauss, M. A., et al. 2008, AJ, 136, 2373
Ricci, C., Bauer, F. E., Arevalo, P., et al. 2016, ApJ, 820, 5
Ricci, C., Trakhtenbrot, B., Koss, M. J., et al. 2017a, ApJS, 233, 17
Ricci, C., Trakhtenbrot, B., Koss, M. J., et al. 2017b, Natur, 549, 488
Risaliti, G., Elvis, M., Fabbiano, G., Baldi, A., & Zezas, A. 2005, ApJL, 623, L93
Schawinski, K., Koss, M., Berney, S., & Sartori, L. F. 2015, MNRAS, 451, 2517
Shen, Y., & Ho, L. C. 2014, Natur, 513, 210
Shu, X. W., Yaqoob, T., & Wang, J. X. 2010, ApJS, 187, 581
Stern, D. 2015, ApJ, 807, 129
Stern, D., McKernan, B., Graham, M. J., et al. 2018, ApJ, 864, 27
Vignali, C., Alexander, D. M., & Comastri, A. 2006, MNRAS, 373, 321
Vignali, C., Alexander, D. M., Gilli, R., & Pozzi, F. 2010, MNRAS, 404, 48
Wachter, K., Leach, R., & Kellogg, E. 1979, ApJ, 230, 274
Wright, E. L., Eisenhardt, P. R. M., Mainzer, A. K., et al. 2010, AJ, 140, 1868
Wu, J., Brandt, W. N., Anderson, S. F., et al. 2012, ApJ, 747, 10
Yuan, S., Strauss, M. A., & Zakamska, N. L. 2016, MNRAS, 462, 1603